JOURNAL OF MATERIALS SCIENCE 25 (1990) 499–505

Hygrothermal effects on structural stiffness and structural damping of laminated composites

HACENE BOUADI, C. T. SUN
Department of Engineering Sciences, University of Florida, Gainesville, Florida 32611, USA

In this paper the hygrothermal effects on structural stiffness and damping of laminated composites are investigated. Since the hygrothermal influence on properties of composite materials is primarily matrix dominated, we first determine experimentally the effects of temperature and moisture on the storage modulus, Poisson's ratio and material damping of the epoxy matrix. With the experimentally determined properties of the epoxy material, we then determine the complex moduli (E_L^*, E_T^*, G_{LT}^* and ν_{LT}^*) of unidirectional glass–epoxy and graphite–epoxy composites. The structural stiffness (extensional and flexural) and damping of symmetric angle-ply laminates of glass–epoxy and graphite–epoxy are then investigated both analytically and experimentally for temperatues of 20° C and 80° C, respectively. Three moisture contents which are the dry, saturated and a non-uniform moisture gradient states corresponding to each temperature case are considered. Numerical and limited experimental results show that the effects of moisture on the real part of A_{11}^*, A_{66}^*, D_{11}^* and D_{66}^* at room temperature, 20° C, are negligible for all the considered cases. But as temperature increases, the moisture and temperature combined influence induces significant changes in the complex stiffness $A_{11}^* A_{66}^*$, D_{11}^* and D_{66}^* especially for the matrix dominated terms.

1. Introduction

Shen and Springer [1] investigated the environmental effects on the elastic moduli of a graphite–epoxy composite and made a survey of existing data showing the effects of temperature and moisture on the elastic modulus of several composites. Their conclusions are listed below.

(i) The hygrothermal effects on the 0° fibre direction laminates are negligible.

(ii) For 90° fibre direction laminates, the hygrothermal effects on the modulus are insignificant in the 200 K to 300 K temperature range. But, between 300 K and 450 K, the hygrothermal effects on the modulus are important.

Putter, Buchanan and Rehfield [2] investigated the influence of frequency and environmental conditions on the dynamic behaviour of graphite–epoxy composites. Their overall conclusions were:

(i) The effects of frequency on the modulus and damping are quite small in all cases.

(ii) The effects of frequency on the modulus and damping are relatively greater for matrix-controlled laminates at higher frequencies (about 400 Hz).

(iii) At the same temperature, damping increases with moisture saturation. But for dry laminates, damping decreases slightly as temperature increases.

From all these experimental works, a general summary can be drawn: the influence of hygrothermal conditions on the elastic modulus, dynamic modulus and damping of composites is matrix dominated.

2. Hygrothermal effects on epoxy matrix

Since the hygrothermal influence on composite properties is matrix controlled [1, 2], the fibre properties are assumed to be constant at any temperature below the glass transition temperature and at any moisture content. Therefore, to obtain the values of the complex moduli of composites, it is sufficient to know how temperature and moisture affect the complex moduli of the epoxy matrix, and then use the micromechanics formulations [3]. Thus, only the following functions need to be experimentally evaluated:

$$\begin{aligned} E'_m &= E'_m(T, c) \\ \nu'_m &= \nu'_m(T, c) \\ \eta_m &= \eta_m(T, c) \end{aligned} \quad (1)$$

The constant fibre properties are given in Table I. The effects of frequency are negligible below 400 Hz. The results of this investigation are not accurate for higher frequencies since their effects have not been taken into account.

The qualitative influence of temperature only on the storage modulus, real part of Poisson's ratio, and damping of epoxy is illustrated in Figs 1–3. There are three distinct regions. At room temperature (in the

TABLE I Properties of glass and graphite fibres

	Glass	Graphite
$E'_{f_{11}}$ (GPa)	70.0	220.0
$E'_{f_{22}}$ (GPa)	70.0	16.6
$G'_{f_{12}}$ (GPa)	28.7	8.27
η_f	0.0015	0.0015
$\nu_{f_{12}}$	0.22	0.16
ϱ (g cm^{-3})	2.60	1.75

0022–2461/90 $03.00 + .12

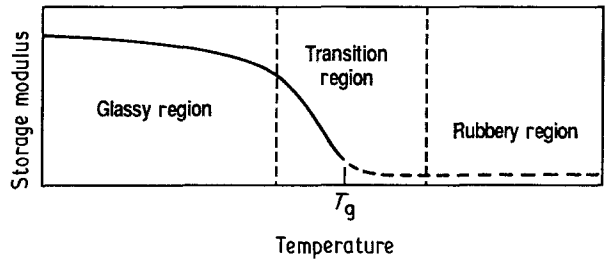

Figure 1 Schematic variation of the storage modulus of epoxy with temperature.

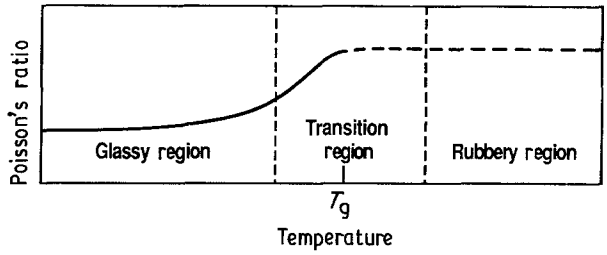

Figure 2 Schematic variation of Poisson's ratio of epoxy temperature.

glassy region), the storage modulus, Poisson's ratio, and damping of epoxy are equal to about 4.0 GPa, 0.35, and 0.018, respectively. In the glassy region, the storage modulus decreases slowly, while Poisson's ratio and the damping increase as temperature increases. In the next region (transition region), the storage modulus decreases rapidly, and both Poisson's ratio and damping reach their maximum values. The last region is the rubbery region where the modulus takes a very low value, and all three parameters stay relatively constant.

Typical values of the modulus in the rubbery region could be 10^{-2} times the glassy modulus or lower. The damping can reach a value of 1 or even 2 in the transition region [4]. Poisson's ratio reaches the limiting value of 0.5, which is approximated by incompressible rubbers [5].

The position of the transition region depends on the moisture concentration. The effects of moisture on the glass transition temperature, T_g, of six epoxy resins have been determined by DeIasi and Whiteside [6]. These results are plotted in Fig. 4. They are comparable with the data of McKague [7] and satisfy the theoretical relation derived in [8].

3. Modelling of epoxy properties

The observations of the preceding section are used for modelling the material properties of epoxy that are given by Equation 1.

The glass transition region of epoxy resin is not

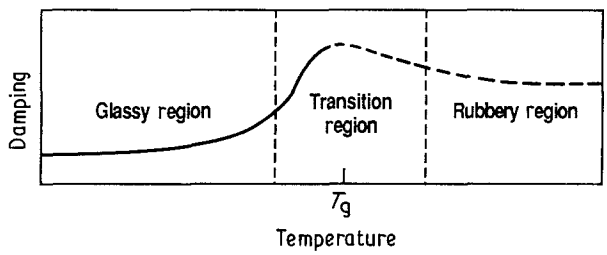

Figure 3 Schematic variation of damping of epoxy with temperature.

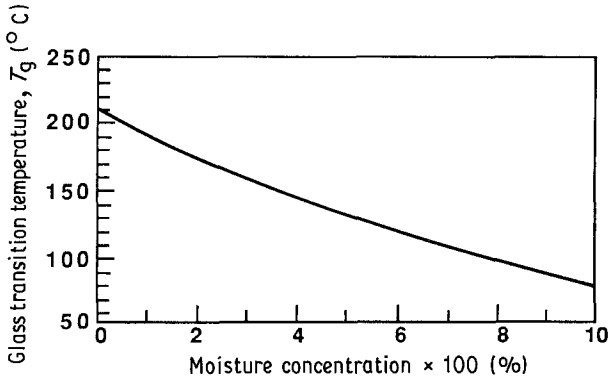

Figure 4 Glass transition temperature of epoxy. From DeIasi and Whiteside [6].

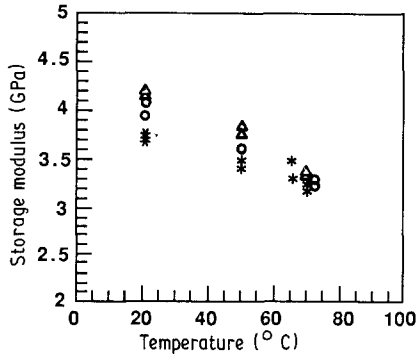

Figure 5 Experimental data of the storage modulus of epoxy as a function of temperature at diverse constant moisture contents. (△) M = 0.0%, (*) M = 2.90%, (○) M = 3.70%.

broad [6], therefore, a glass transition temperature is used instead. The temperature T_g is usually obtained by measuring the expansion of a specimen as function of temperature. The point where the epoxy stops expanding as temperature increases corresponds to the first deviation from the glassy state and is termed T_g.

According to the experimental data [6] plotted in Fig. 4, T_g is strongly dependent on absorbed moisture. These results show that, as the moisture content of epoxy increases, the transition temperature moves to the left in Figs 1–3. Hence, the abrupt change of the material properties starts at a lower temperature as the moisture content increases. This fact and the conclusions reached by previous investigators [4] suggest that the following modelings of E_m^*, ν_m^* and η_m^* are appropriate.

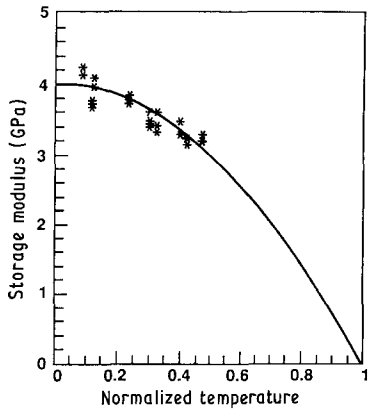

Figure 6 Experimental data of the storage modulus of epoxy as a function of normalized temperature $(T - T_0)/(T_g - T_0)$. (*) Experimental data, (——) Fit to data.

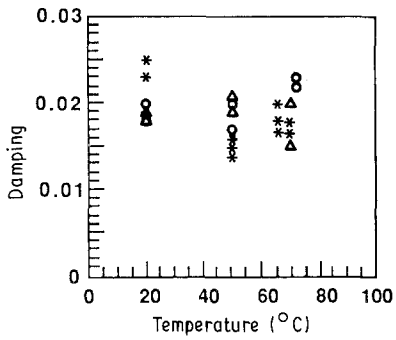

Figure 7 Experimental data of damping of epoxy as a function of temperature at diverse constant moisture contents. (△) M = 0.0%, (*) M = 2.90%, (○) M = 3.70%.

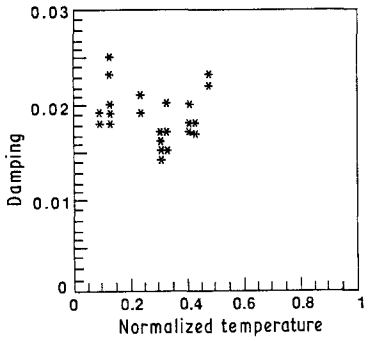

Figure 8 Experimental data of damping of epoxy as a function of normalized temperature $(T - T_0)/(T_g - T_0)$. (*) Experimental data.

$$E'_m = E'_0 \, f\left(\frac{T - T_0}{T_g - T_0}\right) \quad (2)$$

$$\nu'_m = \nu'_0 \, g\left(\frac{T - T_0}{T_g - T_0}\right) \quad (3)$$

$$\eta'_m = \eta'_0 \, h\left(\frac{T - T_0}{T_g - T_0}\right) \quad (4)$$

where the temperature T_0 is equal to 273 K. The moisture concentration appears implicitly in T_g. The glass transition temperature is represented by

$$T_g = 210 \exp(-9c) \quad (\text{in } ^\circ\text{C}) \quad (5)$$

where c is the moisture concentration.

This modelling has been chosen so that it does not represent the material properties beyond T_g, since the study of epoxy in the rubbery stage is not within the scope of this research. Equations 2–4 are valid only for the continuous parts of the curves plotted in Figs 1–3.

4. Experimental results

The experimental investigation is carried out in a Thermotron environment chamber. The storage modulus and material damping of a beam specimen are measured with the impulse hammer technique along with a Fast Fourier Transform analyzer (HP-5420A). The specimen is clamped inside the testing chamber so that the temperature and humidity are maintained at the desired values. More detailed experimental procedures in environmental and damping tests are documented in [9] and [10], respectively.

All test specimens are conditions in a constant relative humidity environment until moisture equilibrium is reached. Then the specimens undergo the impulse hammer technique and the four-point flexure tests to determine the storage moduli, the material damping, and Poisson's ratio at several temperature and moisture contents.

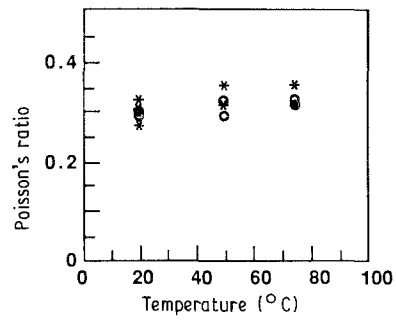

Figure 9 Experiment data of Poisson's ratio of epoxy in terms of temperature. (*) M = 0.0%, (○) M = 4.17%.

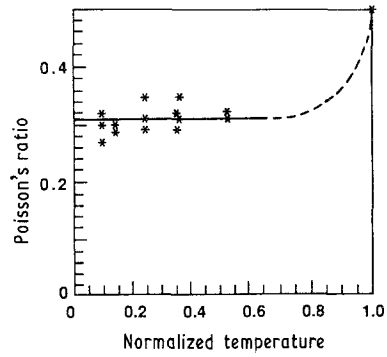

Figure 10 Experimental data of Poisson's ratio in terms of the normalized temperature $T_n = (T - T_0)/(T_g - T_0)$. (*) Experimental data, (——) Fit to data, (– – –) Extrapolation.

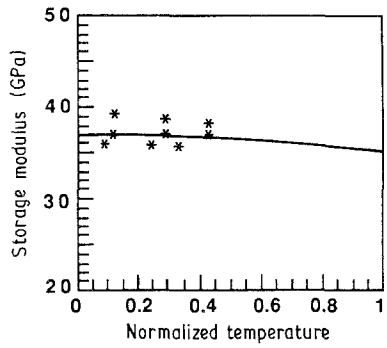

Figure 11 Longitudinal storage modulus (E'_{11}) of glass–epoxy against $T_n = (T - T_0)/(T_g - T_0)$. (——) Theoretical, (*) Experimental data.

4.1. Complex moduli of epoxy

4.1.1. Storage modulus

The experimental data on the storage modulus of epoxy in terms of temperature at three different

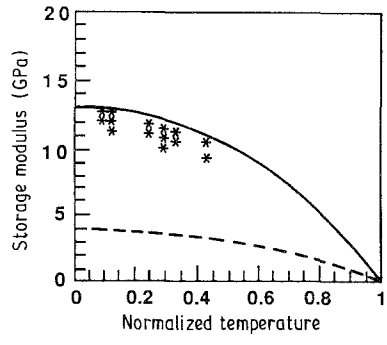

Figure 12 Transverse (E'_{22}) and shear (G'_{12}) storage moduli of glass–epoxy against $T_n = (T - T_0)/(T_g - T_0)$. (——) Theoretical E'_{22}, (*) Experimental E'_{22}, (– – –) Theoretical G'_{12}.

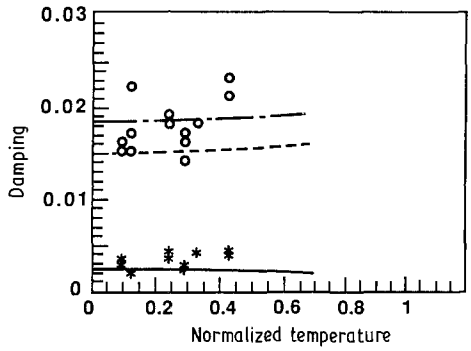

Figure 13 Longitudinal (η_{11}), transverse (η_{22}), and shear (η_g) damping of glass–epoxy against $T_n = (T - T_0)/(T_g - T_0)$. (——) Theoretical η_{11}, (*) Experimental η_{11}, (– – –) Theoretical η_{22}, (○) Experimental η_{22}, (– – –) Theoretical η_g.

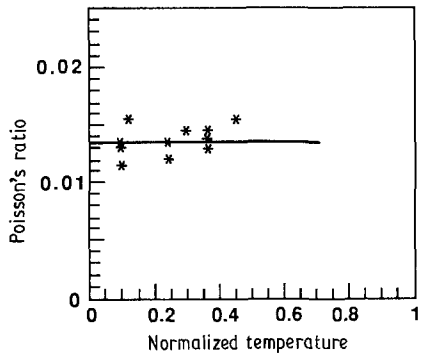

Figure 14 Poisson's ratio (ν'_{12}) of glass–epoxy against $T_n = (T - T_0)/(T_g - T_0)$. (——) Theoretical, (*) Experimental.

equilibrium moisture concentrations are plotted in Fig. 5. It can be concluded that increase in either temperature or moisture content or both results in a decrease in the storage modulus. Representing these results in terms of the following normalized non-dimensional temperature

$$T_n = (T - T_0)/(T_g - T_0) \quad (6)$$

in Fig. 6 shows a clear trend. Experimental studies have shown that the modulus of polymer is very low at the glass transition temperature, therefore, adding the value $E'_m = 0$ for $T = T_g$ to the data yields the following modelling

$$E'_m = 4.0(1 - T_n^2) \quad \text{(GPa)} \quad (7)$$

4.1.2. Material damping

Similarly, the experimental data of the hygrothermal effects on the damping of epoxy are plotted in two Figs (7 and 8). There is very little change in damping for all the considered conditions. Therefore, it is

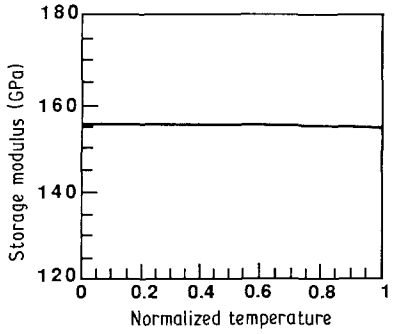

Figure 15 Longitudinal storage modulus (E'_{11}) of graphite/epoxy against $T_n = (T - T_0)/(T_g - T_0)$.

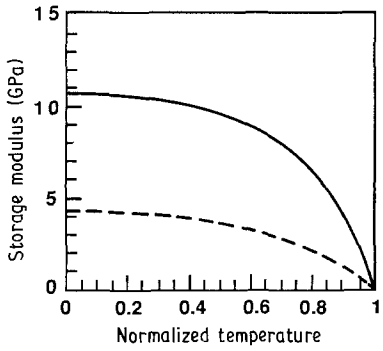

Figure 16 Transverse (E'_{22}) and shear (G'_{12}) storage moduli of graphite–epoxy against $T_n = (T - T_0)/(T_g - T_0)$. (——) Transverse, (– – –) shear.

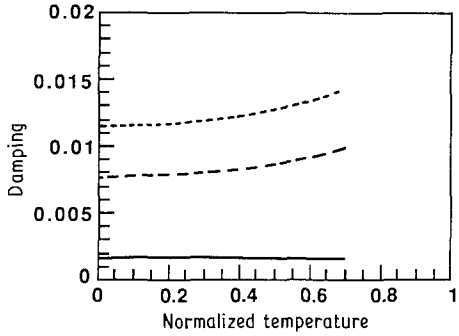

Figure 17 Longitudinal (η_{11}), transverse (η_{22}), and shear (η_G) damping of graphite–epoxy against $T_n = (T - T_0)/(T_g - T_0)$. (——) Longitudinal damping, (– – –) Transverse damping, (– – –) Shear damping.

proposed to let

$$\eta_m = 0.018 \quad (8)$$

for temperatures up to 80° C and moisture contents up to 5%. The conclusion that the hygrothermal effects on the damping of epoxy is negligible is qualitatively corroborated by Putter, Buchanan and Rehfield [2]. A quantitative comparison cannot be made since these researchers have not included in their publication the values of the fibre volume fraction and moisture content of the test specimens.

4.1.3. Poisson's ratio

The experimental values of the Poisson's ratio in terms of temperature at two different moisture contents, are plotted in Fig. 9. These results show that Poisson's ratio increases at a negligible rate as temperature varies from 0 to 80° C.

$$\nu'_m = 0.32 \quad (9)$$

for temperatures up to 80° C and moisture contents up to 5%. Since ν'_m equals 0.5 at the glass transition

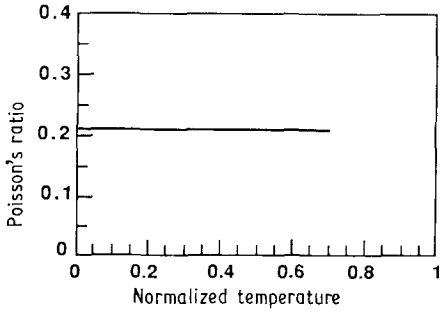

Figure 18 Poisson's ratio (μ'_{12}) of graphite–epoxy against $T_n = (T - T_0)/(T_g - T_0)$. (——) Theoretical.

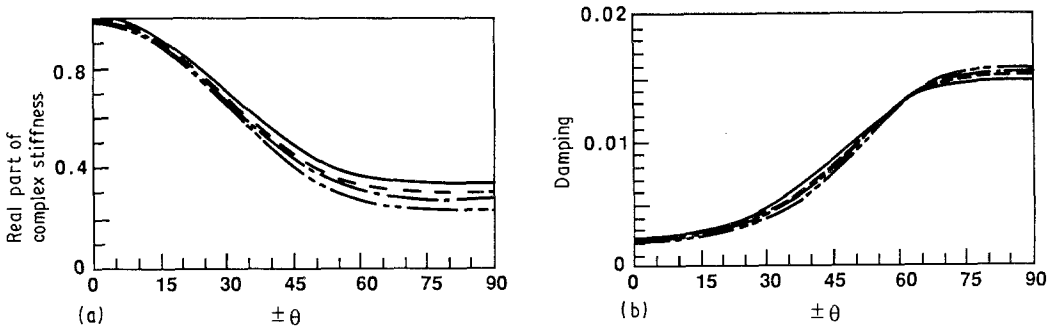

Figure 19 Complex in-plane stiffness A_{11} of glass–epoxy. (a) Non-dimensional real part. (b) Corresponding damping.

Moisture gradient case (A) at 20°C
Moisture gradient case (B) at 20°C
Moisture gradient case (C) at 20°C
Moisture gradient case (A) at 80°C
Moisture gradient case (B) at 80°C
Moisture gradient case (C) at 80°C

Figure 20 Line style legend of Figs 21–27.

temperature ($T_n = 1$), the plot of Poisson's ratio against the normalized temperature has been extrapolated as shown in Fig. 10. The extrapolation displays a qualitative trend only.

4.2. Complex moduli of unidirectional composites

The complex moduli of glass–epoxy and graphite–epoxy in terms of moisture content and temperature can be determined by using the fibres' properties given in Table I, Equations 6–8 and the micromechanics formulas [3].

This procedure is illustrated by determining the storage moduli and the damping of a glass–epoxy lamina with a fibre volume fraction of 0.5 and a graphite–epoxy lamina with a fibre volume fraction of 0.7.

4.2.1. Glass–epoxy

The parameters E'_{11}, E'_{22}, G'_{12}, η_{11}, η_{22}, η_G and ν'_{12} versus the normalized temperature are plotted in Figs 11–14. The experimental data substantiate the theoretical results.

4.2.2. Graphite–epoxy

Similarly, E'_{11}, E'_{22}, G'_{12}, η_{11}, η_{22}, η_G and ν'_{12} against the normalized temperature of graphite–epoxy are plotted in Figs 15–18. For both glass–epoxy and graphite–epoxy, the results show that the matrix-dominated parameters (E'_{22} and G'_{12}) are strongly affected by moisture and temperature, while the fibre-dominated parameters (E'_{11}, ν'_{12}) stay practically constant.

5. Hygrothermal effects on complex structural stiffness of laminated composites

The hygrothermal effects on the in-plane (A^*_{ij}) and the bending (D^*_{ij}) complex stiffnesses of glass–epoxy and graphite–epoxy angle-ply $[(\pm\theta)_2]s$ laminates are investigated. The applied moisture gradients are the cases: A, dry state; B, moisture saturated state; and C, non-uniform moisture gradient state and the uniform applied temperatures of 20° C and 80° C, respectively. The material properties in terms of moisture content and temperature have been determined in Section 4. The fibres' properties are given in Table I. The theoretical expressions of A^*_{11}, A^*_{66}, and D^*_{11}, D^*_{66}, in terms of the fibres and matrix properties have been developed in [11] by using the classical lamination theory and the elastic–viscoelastic correspondence principle.

5.1. Glass–epoxy laminated composites

The fibre volume fraction of the glass–epoxy is 0.5 and the equilibrium moisture content c_∞ is 0.025. Since the fibres do not absorb any moisture, the equilibrium moisture concentration of the matrix is 0.05. The thickness of the laminate is 2.0 mm and A^*_{ij}, and D^*_{ij} are normalized with respect to 75.86×10^{-6} Nm^{-1} and 25.29 Nm, respectively.

The real part of the longitudinal in-plane complex stiffness. A'_{11} and its corresponding damping, $I^{\eta_{11}}$ are plotted in Fig. 19. As the moisture gradients and the temperature change, the relative changes of A'_{11} vary from 6% (for $\theta = 0°$) to 33% (for $\theta = 90°$). Similarly, A'_{66} and $I^{\eta_{66}}$ in Fig. 21. All these cases show that the

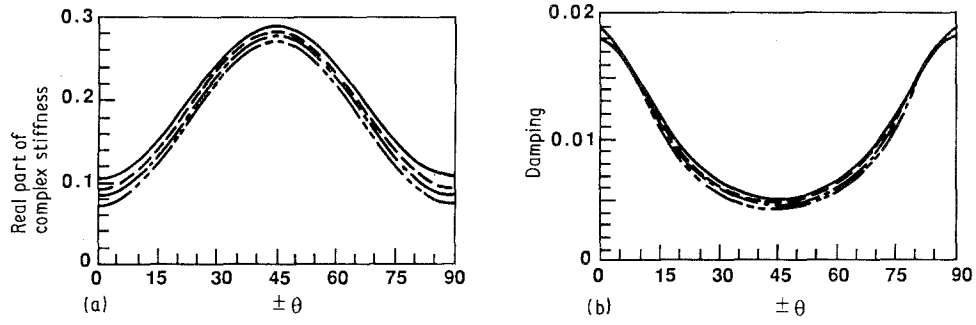

Figure 21 Complex in-plane stiffness A^*_{66} of glass–epoxy. (a) Non-dimensional real part. (b) Corresponding damping.

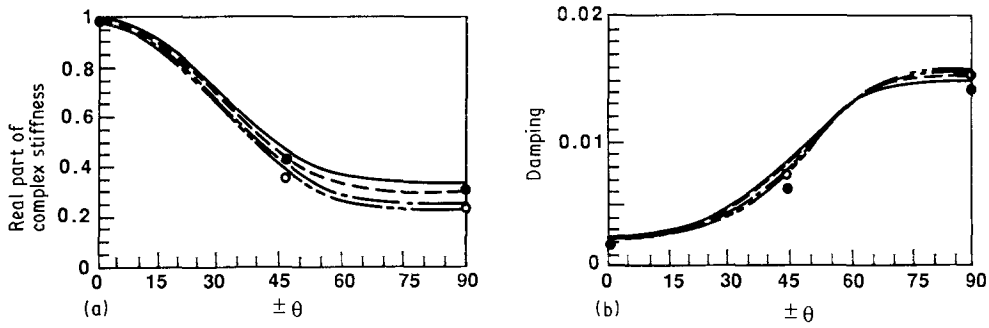

Figure 22 Complex in-plane stiffness D_{11}^* of glass–epoxy. (a) Non-dimensional real part. (b) Corresponding damping. (●) 20° C M = 4%, (○) 80% C M = 4%.

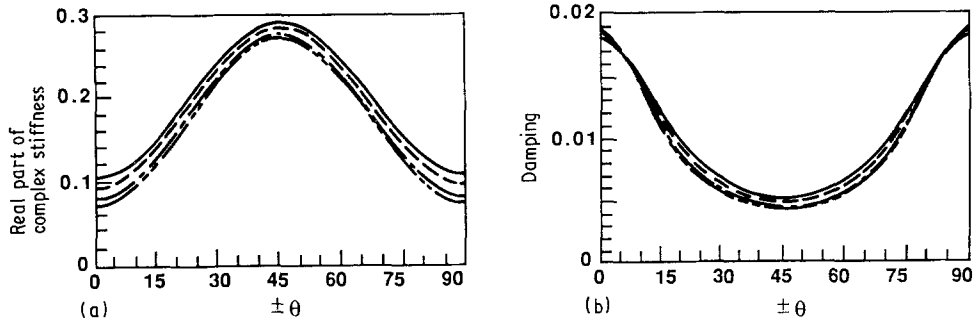

Figure 23 Complex in-plane stiffness D_{66}^* of glass–epoxy. (a) Non-dimensional real part. (b) Corresponding damping.

hygrothermal effects on A_{ij}^* is matrix dominated (the line style legend of the figs is defined in Fig. 20).

The real part of the bending stiffnesses, D_{11}^* and D_{66}^* and their corresponding damping $F^{\eta_{11}}$ and $F^{\eta_{66}}$ are plotted in Figs 22–23. These results yield similar conclusions to those of A_{11}^* and A_{66}^*, respectively. The experimental data of D_{11}' and $F^{\eta_{11}}$ substantiate the theoretical results.

5.2. Graphite–epoxy

The volume fraction of the graphite–epoxy laminate is 0.7 and its equilibrium moisture concentration c_∞ is 0.015. Since all the moisture is absorbed by the matrix, c_∞ of the epoxy is 0.050. The laminate is 2.0 mm thick.

The real parts of the complex stiffnesses (A_{11}', A_{66}', D_{11}' and D_{66}') and their corresponding damping ($I^{\eta_{11}}$, $I^{\eta_{66}}$, $E^{\eta_{11}}$ and $F^{\eta_{66}}$) plotted in Figs 24–27. The terms A_{ij}' and D_{ij}' are normalized with respect to 311.3×10^6 Nm^{-1} and 103.77 Nm, respectively. These results show the same tendency as those of glass–epoxy. Since the volume fraction and the longitudinal modulus of the graphite fibres are higher, the hygrothermal effects are less pronounced.

6. Conclusions

The storage moduli, E_m', are strongly dependent on temperature and moisture content. But, η_m and ν_m' stay constant up to a moisture content M = 5% and a

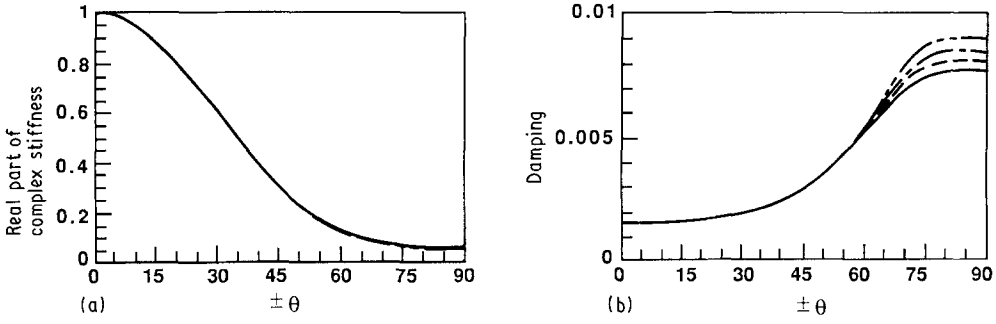

Figure 24 Complex in-plane stiffness A_{11}^* of graphite-epoxy. (a) Non-dimensional real part. (b) Corresponding damping.

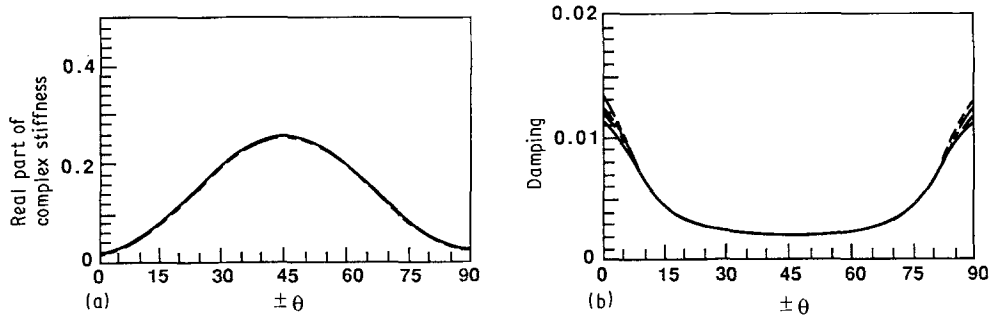

Figure 25 Complex in-plane stiffness A_{66}^* of graphite–epoxy. (a) Non-dimensional real part. (b) Corresponding damping.

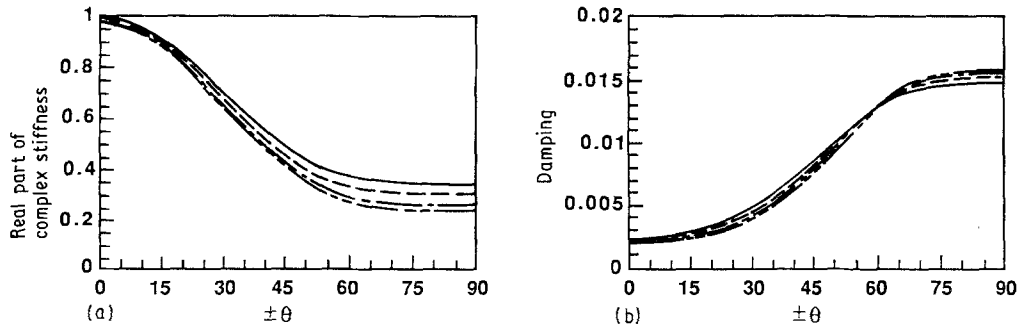

Figure 26 Complex bending stiffness D_{11}^* of graphite–epoxy. (a) Non-dimensional real part. (b) Corresponding damping.

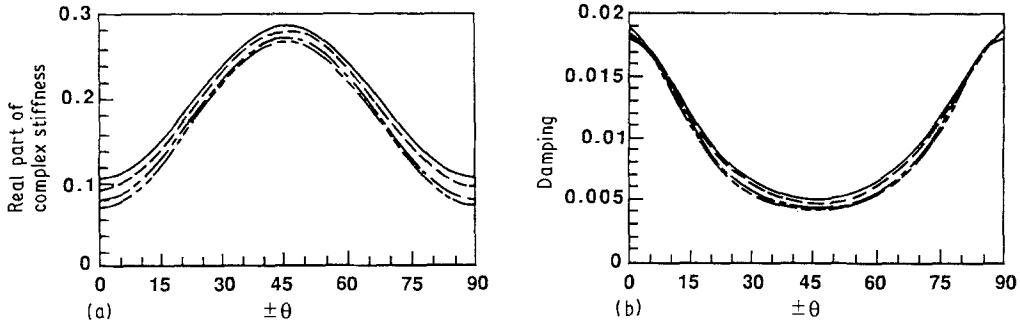

Figure 27 Complex bending stiffness D_{66}^* of graphite–epoxy. (a) Non-dimensional real part. (b) Corresponding damping.

temperature $T = 80°C$. More severe hygrothermal conditions could not be reached in the environmental chamber due to operating temperature limitations of both the chamber and the motion and force transducers used in the impulse hammer technique.

The experimental results of the epoxy properties in combination with the micromechanics formulas are used to determine the hydrothermal effects on the complex moduli of unidirectional glass–epoxy and graphite–epoxy composites. It is shown that only the matrix dominated terms (E'_{22} and G'_{12}) are strongly affected by temperature and/or moisture.

The complex stiffnesses and structural damping of $[(\pm\theta)_2]_S$ glass–epoxy and graphite–epoxy laminates are investigated. These results display the same general trend as those of the complex moduli of unidirectional composites. That is, only the matrix dominated terms are strongly affected by moisture and/or temperature.

Recommendations and additional remarks that arose from this investigation are listed below.

(1) The results and conclusions could vary among different material systems. Hence, it might be necessary to repeat the tests and the methodology for different materials.

(2) The experimental results are valid up to a 80° C temperature and a 5% moisture content. In order to determine the properties of epoxy through a wider range of temperature (from $-50°C$ to 200° C) and moisture content, an environmental chamber and transducers that can operate under more severe hygrothermal conditions need to be used.

References

1. C.-H. SHEN and G. S. SPRINGER, *J. Compos. Mater.* **11** (1977) 250.
2. S. PUTTER, D. L. BUCHANAN and L. W. REHFIELD, ASTM STP 787 (American Society for Testing and Materials, Philadelphia, 1982) pp. 414–424.
3. C. T. SUN, R. F. GIBSON and S. K. CHATURREDI, *J. Mater. Sci.* **20** (1985) 2575.
4. Z. D. NASHIF, D. I. G. JONES and J. P. HENDERSON, "Vibration Damping" (Wiley, New York, 1985) p. 90.
5. L. E. MALVERN, "Introduction to the Mechanics of a Continuous Medium" (Prentice-Hall, New Jersey, 1969) p. 293.
6. R. DEIASI and J. B. WHITESIDE, ASTM STP 658 (1978) pp. 2–20.
7. L. McKAGUE, *ibid.* pp. 193–204.
8. J. J. AKLONIS, W. J. MACKNIGHT and M. SHEN, "Introduction to Polymer Viscoelasticity" (Wiley, New York, 1972) p. 69.
9. H. BOUADI, PhD Thesis, University of Florida, Florida (1978).
10. B. T. LEE, C. T. SUN and D. LIU, *J. Rein. Plast. and Compos.* **6**(2) (1987) 114.
11. C. T. SUN, J. K. WU and R. F. GIBSON, *J. Mater. Sci.* **22** (1987) 1006.

Received 4 March
and accepted 25 July 1988